Available Online: 2 March 2026 DOI: 10.54254/2977-3903/2026.32009

Topology optimization of plate based on the Reissner-Mindlin theory

Yiru Feng

China University of Mining and Technology-Beijing, Beijing, China

13082058155@163.com

Abstract. Current topology optimization of Reissner-Mindlin plates faces dual challenges: the inaccuracy of global stress aggregation in capturing peak stresses and the numerical instability caused by shear locking. This study proposes a rigorous framework that bypasses stress aggregation by enforcing local stress constraints directly via an Augmented Lagrangian (AL) method. To ensure physical fidelity across varying plate thicknesses, we introduce a locking-free polygonal finite element formulation. This approach constructs an assumed shear strain field along element edges, effectively eliminating locking phenomena without relying on reduced integration. The optimization scheme further integrates a vanishing constraint treatment to resolve singularity in low-density regions, with sensitivities computed efficiently via adjoint analysis. Numerical benchmarks demonstrate that the proposed method delivers superior accuracy in peak stress control and robust convergence for both thin and thick plates, offering a scalable solution for stress-critical engineering designs.

Keywords: Reissner-Mindlin plate, topology optimization, augmented lagrangian, polygonal finite elements

1. Introduction

Engineering sectors ranging from aerospace to piping systems rely heavily on flat structural panels. Analysts typically model these components using either Kirchhoff-Love assumptions for thin variations or Reissner-Mindlin kinematics for thicker variants [1]. Modern finite element research aims to treat both regimes within a single robust algorithm. A primary obstacle in unified formulations is the artificial stiffening, or "locking," observed when component thickness decreases relative to the span. While reduced integration resolves this for standard quadrilateral grids, it proves ineffective for general polygonal discretizations [2, 3].

Reduced integration schemes are well known for alleviating locking in standard quadrilateral elements, yet they are generally ineffective when extended to meshes composed of general polygons because the associated shear conditions are not properly satisfied [4, 5]. Polygonal discretizations nonetheless provide notable benefits for representing complex domains and enable more natural element layouts. To exploit these advantages without suffering from locking, dedicated formulations are required [6]. Recent developments have addressed this challenge by defining edge based assumed strain fields derived from Timoshenko beam kinematics [7-9].

Within this numerical setting, topology optimization plays a central role in determining optimal material layouts for objectives such as stiffness enhancement or frequency maximization [10]. The use of polygonal

elements is particularly attractive in this context since they mitigate common numerical artifacts including checkerboard patterns and irregular nodal connectivity [11]. However, incorporating stress limitations into the optimization process remains challenging. Stress constraints tend to dominate regions with low material density, giving rise to the well known singularity issue that obstructs convergence toward physically meaningful solutions [12, 13]. In addition, the inherently local character of stress demands a large constraint set, which significantly increases computational expense.

To address the high cost associated with numerous constraints, global aggregation techniques have traditionally been employed. These methods combine stress responses at the element level into one continuously differentiable quantity, for example through p-norm–type indicators or the Kreisselmeier-Steinhauser function [14-17]. Although such methods have been applied to plate optimization problems for several years, they inherently smooth the stress response and may inadequately capture peak values. Attempts to improve accuracy through element clustering introduce sensitivity to mesh resolution and rely on problem dependent tuning [18, 19].

Recent numerical evidence suggests that local enforcement strategies are more effective for accurately satisfying stress bounds. Active set approaches limit the constraint set to critical regions but remain costly for large scale applications [20, 21]. An alternative is provided by the Augmented Lagrangian framework, which reformulates the constrained problem into a sequence of unconstrained optimizations through penalty and multiplier updates [22-24]. This strategy has demonstrated strong performance and scalability in membrane based optimization problems.

The present work extends the aggregation-free Augmented Lagrangian framework to the topology optimization of Reissner-Mindlin plates using arbitrary polygonal discretizations. By incorporating a locking-free assumed shear strain field and Wachspress interpolants within the PolyStress environment, the proposed method ensures robust performance across varying plate thicknesses. Numerical benchmarks validate the approach's efficiency, demonstrating its ability to generate distinct optimal layouts for both thin and thick plates without the need for mesh-dependent parameter tuning.

2. Theoretical framework and discretization

This section establishes the numerical framework based on the Reissner-Mindlin (RM) plate theory. To address the shear locking phenomenon inherent in thin-plate limits, we propose a polygonal finite element method enhanced with an Assumed Shear Strain (ASS) field.

2.1. Governing equations and discretization

Figure 1 presents an isotropic Reissner-Mindlin plate of thickness h on a domain Ω. The kinematics are defined by the transverse deflection w and the rotation vector θ. Under a transverse load p, the equilibrium implies the balance of bending moments and shear forces:

$$\nabla \cdot (D_b \kappa) + \nabla \cdot (D_s e) + p = 0 \tag{1}$$

where $\kappa = \nabla\theta$ is the curvature vector and $\gamma = \nabla w - \theta$ is the transverse shear strain vector. The constitutive stiffness matrices D_b and D_s are defined explicitly as:

$$\boldsymbol{D}_b = \frac{Eh^3}{12(1-\nu^2)} \begin{bmatrix} 1 & \nu & 0 \\ \nu & 1 & 0 \\ 0 & 0 & \frac{1-\nu}{2} \end{bmatrix}, \quad \boldsymbol{D}_s = \kappa G h \begin{bmatrix} 1 & 0 \\ 0 & 1 \end{bmatrix} \tag{2}$$

Here, E is Young's modulus, ν is Poisson's ratio, $G = E/[2(1+\nu)]$ is the shear modulus, and $\kappa = 5/6$ is the shear correction factor required for the RM model.

The domain Ω is discretized into n_e polygonal elements. By employing Wachspress generalized barycentric coordinates $N_i(x)$ as shape functions, the element displacement field u^e is interpolated from nodal degrees of freedom d_i :

$$u^e(x) = \sum_{i=1}^{n} N_i(x) d_i = N U_e. \tag{3}$$

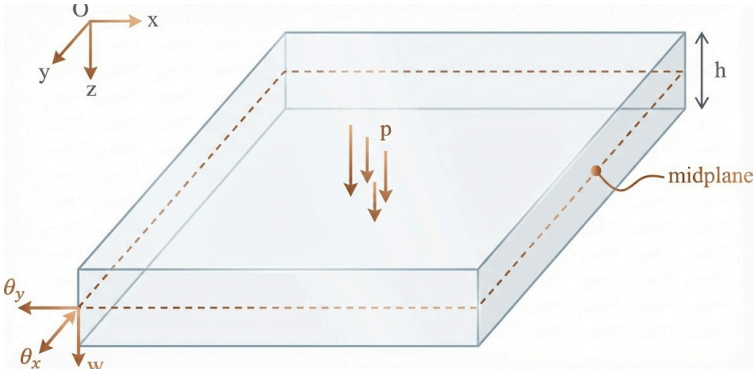

Figure 1. The model of RM plate

2.2. Locking-free assumed shear strain

Directly employing Eqation (2) leads to shear locking as $h \to 0$ due to parasitic shear energy. To circumvent this, we construct an independent Assumed Shear Strain (ASS) field. First, a constant tangential shear strain γ_{t_k} is defined along each element edge k , consistent with the nodal displacements:

$$\gamma_{t_k} = \frac{1}{l_k} \int_{l_k} \left(\frac{\partial w}{\partial s} - \theta_s \right) ds = \frac{w_{k+1} - w_k}{l_k} - \frac{1}{2} \left(\theta_{s,k} + \theta_{s,k+1} \right) \tag{4}$$

Inside the element, the assumed shear field $\tilde{\gamma}$ is approximated linearly using basis functions $P(x)$ and coefficients β :

$$\tilde{\boldsymbol{\gamma}} = \boldsymbol{P}(\boldsymbol{x})\, \beta = \begin{bmatrix} 1 & 0 & x & 0 & 0 & 0 \\ 0 & 1 & 0 & y & 0 & x \\ 0 & 0 & 0 & 0 & 1 & y \end{bmatrix} \beta. \tag{5}$$

The coefficients β are determined by matching the projection of $\tilde{\gamma}$ on the edges with the defined γ_{t_k} via a least-squares fit, yielding the modified shear strain matrix B_s^{AS} :

$$\beta = A^{-1} h(U_e) \to \tilde{\gamma} = B_s^{AS} U_e \tag{6}$$

Consequently, the locking-free element stiffness matrix is assembled by combining the standard bending part with the modified shear part, ensuring robustness across all thickness ratios:

$$K_e = \int_{\Omega_e} B_b^T D_b B_b d\Omega + \int_{\Omega_e} (B_s^{AS})^T D_s B_s^{AS} d\Omega \tag{7}$$

3. Topology optimization via Augmented Lagrangian

This chapter formulates the stress-constrained topology optimization problem. An Augmented Lagrangian (AL) scheme is adopted to effectively handle the large number of local stress constraints and the singularity issues in low-density regions.

3.1. Material model and stress constraints

We utilize the SIMP method with element-wise relative density ρ_e . To ensure mesh independence and clear boundaries, a density filter followed by a Heaviside projection is applied, yielding the physical density $\widetilde{\rho}_e$:

$$\widetilde{\rho}_e = \frac{tanh(\beta_{proj}\eta_h)+tanh(\beta_{proj}(\overline{\rho}_e-\eta_h))}{tanh(\beta_{proj}\eta_h)+tanh(\beta_{proj}(1-\eta_h))} \tag{8}$$

where β_{proj} controls the projection steepness and η_{th} is the threshold (typically 0.5). The local von Mises stress $\sigma_{vm,j}$ for element j is calculated via the stress-displacement matrix DB_j :

$$\sigma_{vm,j} = \sqrt{(DB_j u_j)^T V (DB_j u_j)} \tag{9}$$

To handle the stress singularity in void regions ($\widetilde{\rho}_j \to 0$), we employ the ϵ -relaxation technique (vanishing constraint). The relaxed constraint function g_j is defined such that it is trivially satisfied in voids:

$$g_j = \widetilde{\rho}_j(\frac{\sigma_{vm,j}}{\sigma_{lim}} - 1)^2 + \epsilon^2(\frac{\sigma_{vm,j}}{\sigma_{lim}})^2 - \epsilon^2 \le 0 \tag{10}$$

where ϵ is a small relaxation parameter (e.g., 10^{-3}) ensuring numerical stability when density is zero.

3.2. Optimization problem and solution strategy

The optimization problem aims to minimize volume subject to equilibrium and relaxed stress constraints:

$$s.t. \quad K(\rho)U = F, \quad g_j \le 0 \quad (j = 1, \dots, N) \tag{11}$$

To solve this efficiently, we convert Equation (11) into an unconstrained sub-problem using the Augmented Lagrangian function L :

$$L(\rho, \lambda, \mu) = V + \frac{1}{2\mu} \sum_{j=1}^{N} [max(0, \lambda_j + \mu g_j)^2 - \lambda_j^2] + \frac{\alpha}{2} \left\| \rho - \rho^{old} \right\|^2 \tag{12}$$

where λ are Lagrange multipliers, μ is the penalty parameter, and α is a move-limit damping parameter to stabilize the update. These parameters are updated in an outer loop based on constraint violations:

$$\lambda_j^{k+1} = max(0, \lambda_j^k + \mu^k g_j), \quad \mu^{k+1} = min(\gamma \mu^k, \mu_{max}) \tag{13}$$

3.3. Sensitivity analysis

The derivative of the augmented Lagrangian function L with respect to the design variables is required for the gradient-based optimizer (Method of Moving Asymptotes, MMA). By applying the chain rule to the explicit and implicit dependencies, the total sensitivity is derived as:

$$\frac{\partial L}{\partial \rho_e} = \frac{\partial V}{\partial \rho_e} + \sum_{j \in A} (\lambda_j + \mu g_j)(\frac{\partial g_j}{\partial \rho_e} + (\nabla u_{g_j})^T \frac{\partial U}{\partial \rho_e}) \tag{14}$$

where A denotes the set of active or violated constraints. The term $\partial U / \partial \rho_e$ represents the sensitivity of the displacement field, which is computationally expensive to evaluate directly for every design variable. To avoid this, we employ the Adjoint Method. We introduce an adjoint vector ξ that satisfies the following adjoint equation:

$$K\xi = -\sum_{j \in A} (\lambda_j + \mu g_j) \nabla u_{g_j} \tag{15}$$

where the gradient of the constraint with respect to displacement, ∇u_{g_j} , is derived from Equation (9) and (10):

$$\nabla u_{g_j} = \frac{\partial g_j}{\partial \sigma_{vm}} \frac{1}{\sigma_{vm}} (DB_j)^T V (DB_j) u_j \tag{16}$$

Finally, substituting the adjoint relation into Equation (14) yields the efficient sensitivity formula:

$$\frac{\partial L}{\partial \rho_e} = \frac{\partial V}{\partial \rho_e} + (\lambda_e + \mu g_e)\frac{\partial g_e}{\partial \rho_e} + \xi^T \frac{\partial U}{\partial \rho_e} \tag{17}$$

The explicit derivative $\partial g_e / \partial \rho_e$ captures the direct effect of density changes on the constraint limit, while the adjoint term captures the implicit mechanical redistribution. Standard chain rules apply for the filter and projection steps implicit in $\partial / \partial \rho_e$.

4. Numerical examples

This section applies an augmented Lagrangian strategy to a series of topology optimization examples governed by pointwise stress limits in order to assess the performance of the proposed approach. These studies also establish a basis for future investigations into the structural design of plates composed of multiple materials, layered systems, and direction-dependent properties, which are of both theoretical interest and practical relevance.

4.1. Portal frame

The subsequent benchmark concerns a portal frame structure previously investigated in several studie. The corresponding geometry and applied constraints are illustrated in Figure 2. The computational domain is represented by a mesh of 100,000 polygonal finite elements generated. In this case, the material behavior is assumed to be linear elastic, with a Young's modulus of 100 GPa and a Poisson ratio of 0.25. The allowable stress is specified as 1000 MPa.

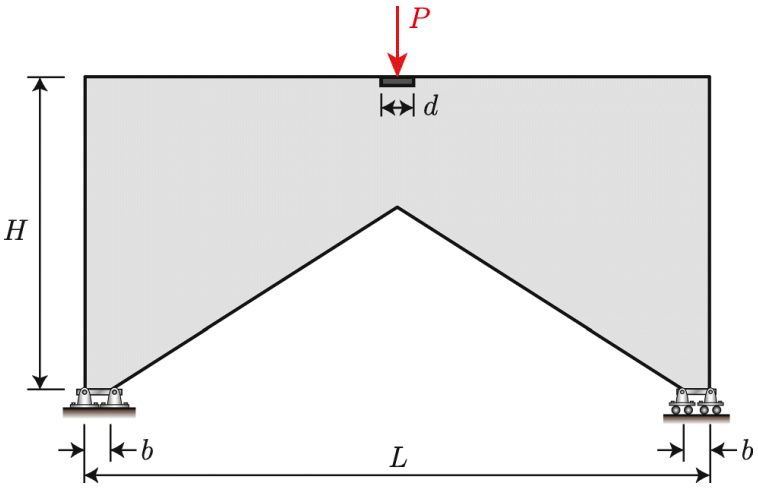

Figure 2. Portal frame domain

In this example, the optimized designs obtained using SIMP and AL as density interpolation schemes are evaluated and contrasted. When applying the AL formulation, the parameter p_0 is chosen as 3.5, as defined in Equation (12). The optimized layouts presented in Figure 3 are generated with a filter length of $R = 0.25$ m. Symmetry with respect to the vertical axis is enforced through the filtering procedure.

Although solutions with near-symmetric characteristics can be produced without explicitly enforcing symmetry, this constraint is introduced because the adopted polygonal discretization does not possess geometric symmetry about the vertical axis. The resulting designs demonstrate that effectively eliminates material in regions associated with elevated stress, particularly near the re-entrant corner located at the lower central portion of the portal frame, for both SIMP- and AL-based solutions. Owing to the strong nonlinearity inherent in stress-limited optimization, the layouts obtained from the two interpolation strategies exhibit

noticeable differences, which is anticipated. The results further confirm that the stress constraints are locally fulfilled, as evidenced by the stress distributions shown in the central and right-hand portions of the figure.

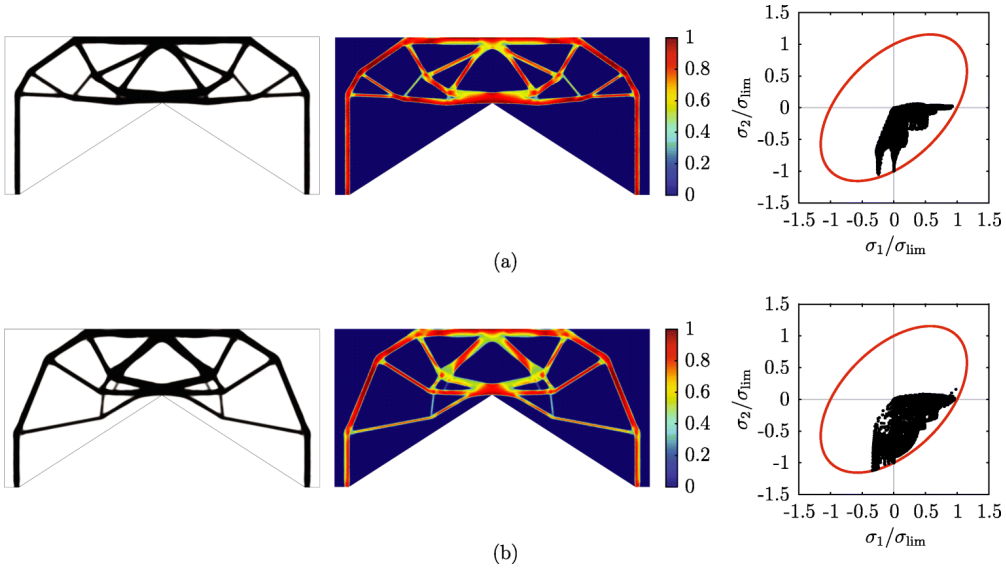

Figure 3. Topology optimization results for the portal frame

4.2. Slender cantilever plate

This set of numerical studies examines rectangular cantilever plates restrained along a single boundary and loaded by a uniform transverse pressure applied to the opposite side. Two benchmark configurations reported in previous studies are considered, with the only distinction being the length-to-width ratio.

Figure 4 presents a benchmark problem originally reported by Goo et al. [17] In this setup, a total load of 0.1 N is evenly applied to three nodes located at the center of the loaded boundary in order to reduce local stress intensification. All translational and rotational degrees of freedom along the fixed edge are fully constrained. Consistent with the reference study, the elastic modulus is taken as 1 GPa and the Poisson ratio is assumed to be 0.3. The geometry of the structure measures 60 mm in length and 20 mm in width, with a plate thickness of 0.5 mm, placing it within the thin-plate regime. The computational domain is discretized using 10,092 standard four-node quadrilateral elements for the numerical implementation.

To further investigate the influence of thickness, additional cantilever plate cases are considered. For the case where the plate is 10 mm in depth and treated as a thick plate, the load level is raised to 10 N so that a similar stress magnitude is obtained. In both thickness scenarios, the allowable stress is limited to 16 MPa, and a density filter with a radius of 5 mm is adopted.

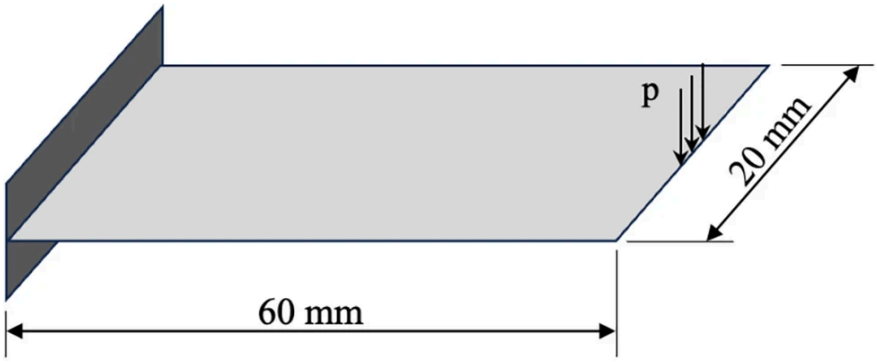

Figure 4. Cantilever plate

The optimized layout obtained for the thin plate is shown in Figure 5(a) and agrees well with the configuration. Stress aggregation strategies, especially those based on a p-norm formulation, are sensitive to the choice of the aggregation parameter, since different values may lead to noticeably different structural layouts. In contrast, the present approach delivers a well-defined solution, although results from alternative formulations may still depend on factors such as discretization density. The resulting equivalent stress field, expressed in nondimensional form, indicates adherence to the allowable stress requirement across the entire region. The optimized design retains roughly 26.5% of the original material volume.

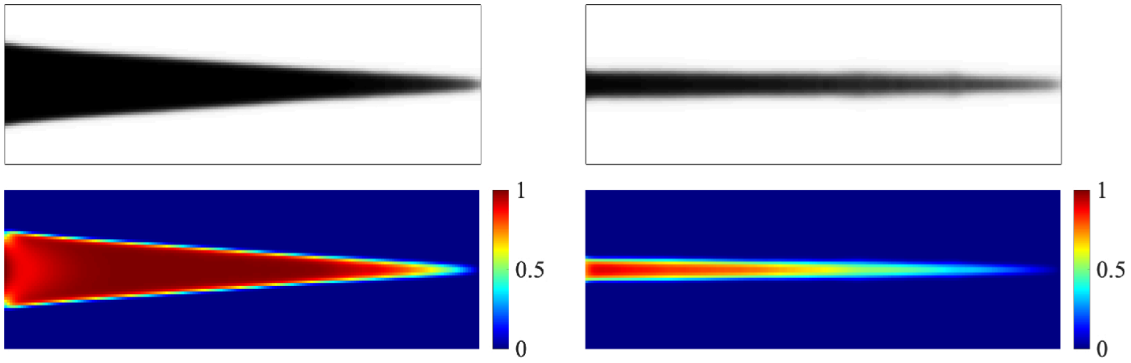

Figure 5. Comparison of the final topology-optimised model with COMSOL

The optimized structure for the thick plate scenario is presented in Figure 5(b). While the overall structural pattern remains comparable to that of the thin plate, the retained material is further reduced to approximately 11.4%. Since the system does not impose fixed numerical constraints, the same computational procedure can be applied directly to both slender and thick configurations without additional adjustments. It should be emphasized that the study was limited to the thin plate case.

For both plate thicknesses, the evolution of the objective function, expressed as the material volume ratio, together with the maximum normalized von Mises stress over successive AL iterations, is illustrated in Figure 6. The results show that the starting design, determined by the initial guess, already complies with the imposed stress limit in each case. Nevertheless, the optimization process remains beneficial, as it enables a systematic balance between reducing material usage and maintaining compliance with the stress constraint.

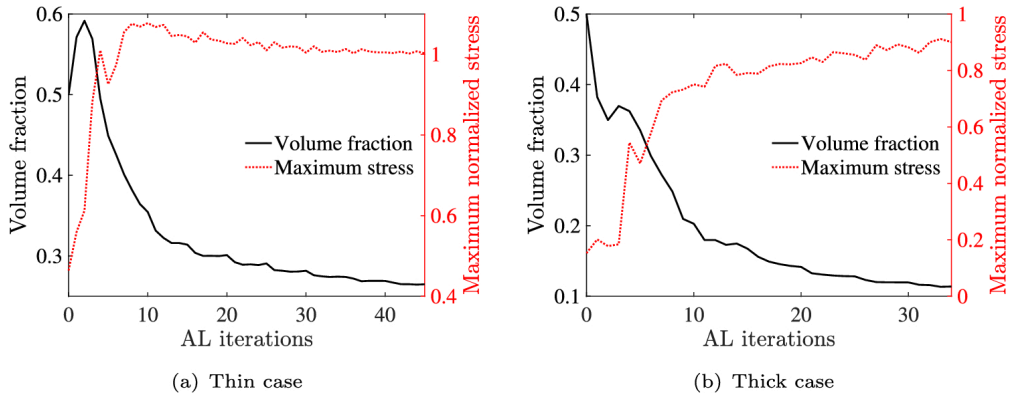

Figure 6. Volume fraction versus stress iteration curve

5. Conclusions

This study establishes a robust topology optimization framework for Reissner–Mindlin plates that explicitly enforces local stress limits without relying on global aggregation. By synergizing a local Augmented Lagrangian strategy with a locking-free polygonal finite element method, the proposed approach ensures precise peak stress control and numerical stability across varying plate thicknesses.

(1) A locking-free Reissner–Mindlin plate formulation was established for general polygonal discretizations using an assumed shear strain field defined along element edges. This construction effectively eliminates shear locking without reduced integration and ensures consistent accuracy across different thickness regimes, while preserving the geometric flexibility of polygonal meshes.

(2) Local stress constraints were enforced directly at the element level through an Augmented Lagrangian formulation combined with a vanishing stress constraint treatment. This strategy removes the need for global stress aggregation, captures peak stresses reliably, and avoids the singularity issues commonly encountered in stress-limited topology optimization.

(3) Numerical investigations on several benchmark problems confirmed that the proposed method produces well-defined and physically meaningful optimal layouts. Compared with conventional aggregation-based and SIMP-type approaches, the present framework exhibits faster convergence and improved stress control, particularly for large-scale problems with a high number of local constraints.

In conclusion, the proposed framework offers a versatile and reliable tool for stress-critical engineering design. Its ability to accommodate complex geometries and operate uniformly across different plate regimes, without reliance on mesh-dependent tuning, renders it highly suitable for practical applications in aerospace, mechanical, and civil structures.

References

[1] Le, V. A. (2017). Reissner-Mindlin plate theory. In *Nonlinear theory of elastic plates* (pp. 67–82). Elsevier. https: //doi.org/10.1016/B978-1-78548-227-4.50004-6

[2] Pham, Q.-H., & Phan, D.-H. (2022). Polygonal topology optimization for Reissner–Mindlin plates. *Engineering with Computers, 38*(Suppl. 1), 141–154. https: //doi.org/10.1007/s00366-020-01047-2

[3] Bendsøe, M. P., & Kikuchi, N. (1988). Generating optimal topologies in structural design using a homogenization method. *Computer Methods in Applied Mechanics and Engineering, 71*(2), 197–224. https: //doi.org/10.1016/0045-7825(88)90086-2

[4] MacNeal, R. (1993). *Finite elements*. CRC Press.

[5] Narayan, S. L., Bombarde, D. S., Gautam, S. S., & Nandy, A. (2023). Comparison of selective reduced integration, enhanced assumed strain and assumed natural strain formulation in alleviating locking. In G. Manik, S. Kalia, O. P. Verma, & T. K. Sharma (Eds.), *Recent advances in mechanical engineering* (pp. 643–654). Springer Nature. https: //doi.org/10.1007/978-981-19-2188-9_58

[6] Nguyen-Xuan, H. (2017). A polygonal finite element method for plate analysis. *Computers & Structures, 188*, 45–62. https: //doi.org/10.1016/j.compstruc.2017.04.002

[7] Katili, I., Maknun, I. J., Katili, A. M., Bordas, S. P. A., & Natarajan, S. (2019). A unified polygonal locking-free thin/thick smoothed plate element. *Composite Structures, 219*, 147–157. https: //doi.org/10.1016/j.compstruct.2019.03.020

[8] Soh, A. K., Long, Z. F., & Cen, S. (1999). A new nine DOF triangular element for analysis of thick and thin plates. *Computational Mechanics, 24*(6), 408–417. https: //doi.org/10.1007/s004660050461

[9] Videla, J., Natarajan, S., & Bordas, S. P. A. (2019). A new locking-free polygonal plate element for thin and thick plates based on Reissner-Mindlin plate theory and assumed shear strain fields. *Computers & Structures, 220*, 32–42. https: //doi.org/10.1016/j.compstruc.2019.04.009

[10] Talischi, C., Paulino, G. H., Pereira, A., & Menezes, I. F. M. (2012). PolyTop: A Matlab implementation of a general topology optimization framework using unstructured polygonal finite element meshes. *Structural and Multidisciplinary Optimization, 45*(3), 329–357. https: //doi.org/10.1007/s00158-011-0696-x

[11] Sved, G., & Ginos, Z. (1968). Structural optimization under multiple loading. *International Journal of Mechanical Sciences, 10*(10), 803–805. https: //doi.org/10.1016/0020-7403(68)90021-0

[12] Kirsch, U. (1990). On singular topologies in optimum structural design. *Structural Optimization, 2*(3), 133–142. https: //doi.org/10.1007/BF01836562

[13] Kirsch, U. (1989). Optimal topologies of truss structures. *Computer Methods in Applied Mechanics and Engineering, 72*(1), 15–28. https: //doi.org/10.1016/0045-7825(89)90119-9

[14] Duysinx, P., & Sigmund, O. (1998). *New developments in handling stress constraints in optimal material distribution* [Paper presentation]. 7th AIAA/USAF/NASA/ISSMO Symposium on Multidisciplinary Analysis and Optimization, St. Louis, MO, United States. https: //doi.org/10.2514/6.1998-4906

[15] Holmberg, E., Torstenfelt, B., & Klarbring, A. (2013). Stress constrained topology optimization. *Structural and Multidisciplinary Optimization, 48*(1), 33–47. https: //doi.org/10.1007/s00158-012-0880-7

[16] Kiyono, C. Y., Vatanabe, S. L., Silva, E. C. N., & Reddy, J. N. (2016). A new multi-p-norm formulation approach for stress-based topology optimization design. *Composite Structures, 156*, 10–19. https: //doi.org/10.1016/j.compstruct.2016.05.058

[17] Le, C., Norato, J., Bruns, T., Ha, C., & Tortorelli, D. (2010). Stress-based topology optimization for continua. *Structural and Multidisciplinary Optimization, 41*(4), 605–620. https: //doi.org/10.1007/s00158-009-0440-y

[18] Liu, H., Yang, D., Hao, P., & Zhu, X. (2018). Isogeometric analysis based topology optimization design with global stress constraint. *Computer Methods in Applied Mechanics and Engineering, 342*, 625–652. https: //doi.org/10.1016/j.cma.2018.08.013

[19] Zhang, W., Jiang, S., Liu, C., Li, D., Kang, P., Youn, S.-K., & Guo, X. (2020). Stress-related topology optimization of shell structures using IGA/TSA-based Moving Morphable Void (MMV) approach. *Computer Methods in Applied Mechanics and Engineering, 366*, Article 113036. https: //doi.org/10.1016/j.cma.2020.113036

[20] Guo, X., Zhang, W. S., Wang, M. Y., & Wei, P. (2011). Stress-related topology optimization via level set approach. *Computer Methods in Applied Mechanics and Engineering, 200*(47–48), 3439–3452. https: //doi.org/10.1016/j.cma.2011.08.016

[21] da Silva, G. A., Aage, N., Beck, A. T., & Sigmund, O. (2021). Local versus global stress constraint strategies in topology optimization: A comparative study. *International Journal for Numerical Methods in Engineering, 122*(21), 6003–6036. https: //doi.org/10.1002/nme.6781

[22] Bruggi, M., & Duysinx, P. (2012). Topology optimization for minimum weight with compliance and stress constraints. *Structural and Multidisciplinary Optimization, 46*(3), 369–384. https: //doi.org/10.1007/s00158-012-0759-7

[23] Pereira, J. T., Fancello, E. A., & Barcellos, C. S. (2004). Topology optimization of continuum structures with material failure constraints. *Structural and Multidisciplinary Optimization, 26*(1–2), 50–66. https: //doi.org/10.1007/s00158-003-0301-z

[24] Emmendoerfer, H., & Fancello, E. A. (2014). A level set approach for topology optimization with local stress constraints. *International Journal for Numerical Methods in Engineering, 99*(2), 129–156. https: //doi.org/10.1002/nme.4676